MODELING SINGLE EVENT UPSETS IN FLOATING GATE MEMORY CELLS

Nauman Z. Butt and Muhammad Alam
School of Electrical and Computer Engineering, Purdue University, West Lafayette, IN 47906
765-494-9733; e-mail: nbutt@purude.edu

ABSTRACT

We model soft errors in Floating Gate (FG) memory cells due to charge loss after single radiation particle strikes. In contrast to various classical models, we show that the transient carrier flux over the oxide barriers coming into and out of the floating gate from high energy tail of the generated carriers can be the dominant mechanism of charge loss. We use this model to quantify the single event upset (SEU) susceptibility of FG memory technologies for cosmic ray neutrons and alpha particle strikes. We predict that the SEU sensitivity of FG memory cells will significantly increase with future cell scaling. [*Keywords:* FG memory, Scaling, Single event upset, Transient carrier flux.]

INTRODUCTION

Floating gate (FG) memories, in particular the Flash memory is undergoing rapid advancements in performance, scaling, and the total memory size [1-3]. The cell area in Flash memory has been scaling down by about 50% at each generation for the last decade [3, 4]. The multi-level-cell (MLC) technology promises to further increase the bit density by a factor of *n*, with *n* being the number of bits/cell. This rapid scaling of Flash memory has however increased the challenges regarding the reliability and endurance of the cell. In past, the reliability of a Flash memory array has almost exclusively been related to the wear out of the tunnel oxide with program/erase cycling. Such wear out occurs because the injection of high energy carriers in a Fowler-Nordheim or hot carrier stress creates new traps or defects in the tunnel oxide which results in charge loss due to a well-known phenomenon of Stress-Induced-Leakage-Current (SILC) [1]. This imposes a limit on the tunnel oxide scaling and on the maximum oxide electric field. Moreover, the number of stored charges in the FG is dramatically reduced for each NAND flash generation by ~ x0.77. The current generations of NAND flash cells store approximately 1000 or fewer electrons in the programmed state [4]. The tolerance of charge loss is therefore decreasing rapidly with technology generations, further increasing the challenge for the reliable cell operation.

Until recently, the effects of radiation in Flash memories have mainly been a concern for the space or aircraft applications [5]. The heavy ions and other high energy particles which are abundantly present at altitudes far above the sea-level cause a variety of problems including the soft errors (mainly SEU and Single-Event-Functional-Interrupts (SEFI)) and hard errors pertaining to oxide degradation due to total dose. Recent experiments on current generation Flash memories [6-8] have however shown that significant amount of radiation effects can be observed at the sea-level or terrestrial environments. Previously, the most sensitive component of Flash memory used to be the control circuitry for sense amplifiers and charge pumps. The FG cell array on the other hand was considered to be relatively insensitive to radiation strikes at least at terrestrial levels. This is however changing rapidly because with only ~1000 or fewer electrons stored in the FG, the cells have now become sensitive to charge deposited by the terrestrial cosmic ray neutrons and alpha particles.

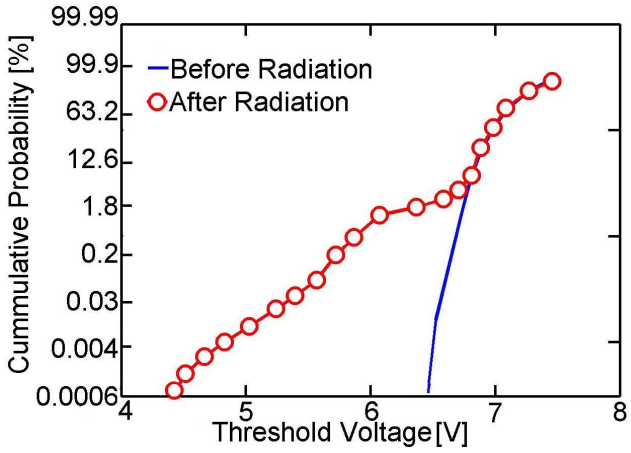

Fig. 1 Cumulative probability distribution of threshold voltages in a programmed FG array before and after irradiation with heavy ions (taken from Ref. [5]). The distribution before irradiation is a tight Gaussian whereas the distribution after irradiation shows a secondary peak due to the cells disturbed by the particle strikes.

The SEU in Flash cell arrays have been demonstrated by Cellere *et al* and others in several different contributions [5, 6, 9-16]. In Fig. 1 we show one of the data on a programmed FG array after heavy ions irradiation taken from Ref [5]. The cumulative probability distribution of threshold voltages (V_{th}) in the array during the programmed state is plotted before and immediately after irradiation by Iodine ions. V_{th} in a cell is directly proportional to the number of stored electrons and the oxide electric field (E_{ox}) [1]. For the non-irradiated array, V_{th} distribution has a form of tight Gaussian. In the case of the irradiated devices, there is a secondary peak in the distribution corresponding to the percentage of cells hit by the ions. The secondary peak in the V_{th} distribution is due to the loss of stored electrons (ΔQ) from the FG due to irradiation. The shift in threshold voltage is given by: $\Delta V_{th} = \Delta Q / C_{PP}$, where C_{PP} is the FG-CG capacitance. This reduces the noise margin between the programmed and the erased states. The SEU occurs when ΔV_{th} becomes greater than the noise margin. If ΔV_{th} is smaller than the noise margin then there is no SEU immediately, however the charge loss tolerance of the cell drops down which can cause retention problems.

This paper is organized in seven sections. Section I is the introduction and Section II describes the existing models and their limitations. Section III explains our theoretical model while Section IV discusses numerical simulations used to validate the proposed model. We analyze results in Section V and discuss some of the trends in Section VI. Finally conclusions are provided in Section VII.

II. EXISTING MODELS

There are several proposed mechanisms of the observed charge loss from the FG as illustrated in Fig. 2. Here we briefly describe some of the earlier proposed mechanisms along with their strengths and limitations:

978-1-4244-2050-6/08/$25.00 ©2008 IEEE

IEEE CFP08RPS-CDR 46th Annual International Reliability Physics Symposium, Phoenix, 2008

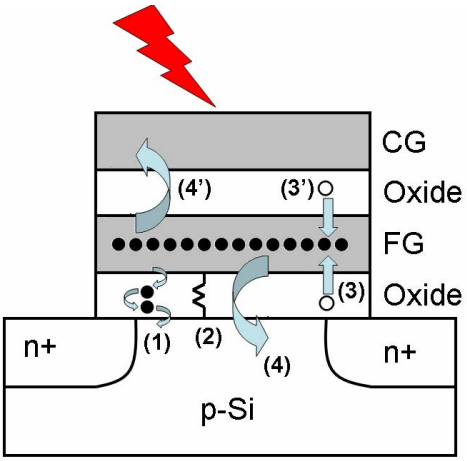

Fig. 2 Different models of FG charge loss due to a radiation particle strike are illustrated in the cross-section of a FG memory cell and denoted by numbers. (1) stands for trap-assisted-tunneling (TAT) model, (2) illustrates the conductive pipe model (3 and 3') represents the model in which holes generated in the oxides move into FG escaping the prompt recombination in oxides and (4 and 4') illustrates the electron emission model.

1) Trap Assisted Tunneling (TAT): The radiation strike creates defects in the tunnel oxide which can provide a percolation path for electrons to tunnel through the tunnel oxide. This mechanism is called trap assisted tunneling (TAT) and is in fact a major cause of oxide wear out due to electrical stresses from program/erased cycling [1]. For irradiated devices, TAT has been shown to cause retention problems in at least some percentage of devices hit by radiation. TAT however takes a long time to discharge a FG cell (several hours to weeks) [15]. The SEU data (e.g. Fig. 1) on the other hand is taken immediately after irradiation and does not change with time afterwards. This makes it clear that TAT cannot be responsible for SEU in FG cells, although it can result in hard errors causing retention problems.

2) Conductive Pipe Model: The dense plasma of e-h pairs creates a very thin (~10nm) transient conductive path in the tunnel oxide for a sub pico-second time after the strike. This is accompanied by the local lowering of oxide energy barrier which enables the stored FG electrons to flow out through the conductive pipe. This model was proposed by Cellere *et al* for explaining charge loss due to heavy ion strikes [11, 15]. Although this phenomenological model can fit the experimental charge loss data well, there is lack in physical details of the mechanisms governing the path resistance and the oxide barrier lowering.

3) Generation/Recombination/Transport in Oxide: Some of the hot holes generated in the tunnel oxide or inter-poly dielectric that survive the prompt recombination phase [17] can drift into the FG, where they recombine with the stored electrons, thus reducing the FG negative charge. Indeed, the negative charge on the FG itself produces the oxide fields attracting the holes. On the other hand, the radiation generated electrons are driven toward bulk Si or CG within very short times due to their superior mobility. The problem with this model is that it does not match quantitatively with the charge loss data taken on FG Flash memory cells [15]. The number of holes that survive the prompt recombination after a heavy ion strike in a 10 nm tunnel oxide is less than 100 whereas data shows that charge loss is a few thousand electrons.

4) Electron Emission: Electrons stored in the FG can gain energy from the ionizing radiation and be emitted over the oxide barrier height toward the CG or the substrate. This mechanism is also called photo-emission. It was originally proposed by Snyder *et al* as one of the mechanism of charge loss in FG EEPROM cells under gamma ray irradiation [18]. The emission over the oxide was empirically modeled. There has however been no attempt in our knowledge to physically model this mechanism or to extend it for heavy ions or other particles strikes. Moreover, in this model, photoemission is *only* limited to the stored FG electrons which has no physical justification. In fact, a particle strike can generate a much larger number of electrons compared to the *net* stored FG electrons, and a portion of them can be energetic enough to be emitted over the oxide barriers.

From the above discussion it is evident that the cause of charge loss from FG cells leading to SEU is not fully understood. The traditional models like (3) fail to quantitatively predict the charge loss whereas some newly developed models like (2) lack the physical details of the involved mechanisms. In this paper we provide a new physics based model which matches with the trends and quantitative values of charge loss found in experiments reasonably well.

III. Transient Carrier Flux (TCF) Model

We propose that the *net* flux of hot carriers passing over the oxide barriers within a short time (~ psec) at the FG/oxide interfaces can be the dominant mechanism of FG charge loss in a single event strike. This Transient-Carrier-Flux (TCF) model is illustrated in Fig. 3. The energy band profiles of conduction and valence bands along the vertical axis of the FG cell through the gate stack are plotted in the programmed state of the cell. Fig. 3 also shows the energy distributions of the generated electrons and holes in FG, CG and substrate regions of the cell shortly after the strike. (We will discuss the details of shape and dynamics of energy distributions in Section III). The electrons and holes fluxes into and out of the FG coming from tail of the transient carrier distributions are depicted by the arrows. In the case of zero oxide electric field, the incoming and outgoing carrier flux balances each other at both FG/oxide interfaces and hence the net flux is zero. In the programmed state however, there is relatively high oxide electric field due to the electrons stored in the FG. Because of this electric field, the outgoing FG electron flux is greater than the incoming electron flux. Moreover, the incoming holes flux is greater than the outgoing FG holes flux. The net flux therefore results in a reduction of stored electrons in the FG.

In a 50 nm thick FG, an alpha particle generates approximately 4500 e-h pairs, while a secondary fragment created by cosmic ray neutron strike can deposit 15000-45000 e-h pairs in the same thickness [17]. On the other hand, current FG memory cells typically store less than 1000 electrons to obtain the required programming window between the two states [3]. A small imbalance between the inward and outward FG flux can hence be significant to disturb the cell state where the charge loss tolerance may be 100 or fewer electrons. The net electron (hole) flux out of the FG is:

$$J_{e(h),FG}(t) = J^{+}_{e(h),FG}(t) - J^{-}_{e(h),FG}(t), \qquad (1a)$$

where

$$J^{+}_{e(h),FG}(t) = J_{e(h),CG\to FG}(t) + J_{e(h),Sub\to FG}(t) \qquad (1b)$$

$$J^{-}_{e(h),FG}(t) = J_{e(h),FG\to CG}(t) + J_{e(h),FG\to Sub}(t) \qquad (1c)$$

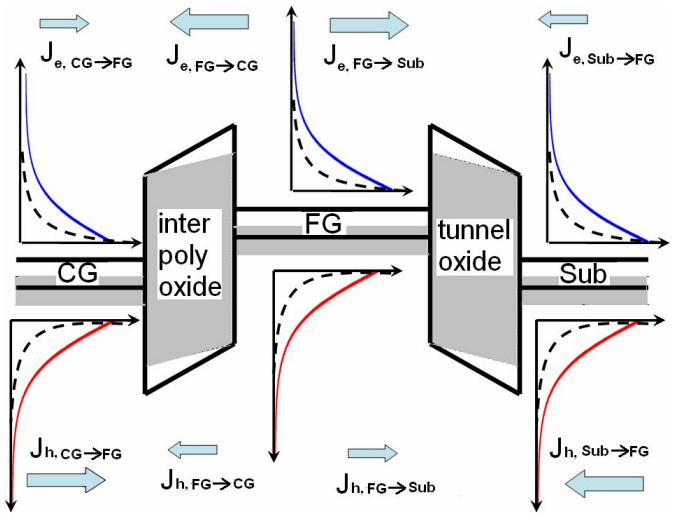

Fig. 3 Energy band profiles along the vertical axis through the gate stack of a FG cell in programmed state. The energy distributions of e-h pairs generated by a particle strike in CG, FG and substrate regions and carrier fluxes into and out of the FG are illustrated.

In above equations, $J_{e(h),FG\to CG}$ and $J_{e(h),FG\to Sub}$ are the outward FG electron (hole) flux to CG and substrate respectively, whereas $J_{e(h),CG\to FG}$ and $J_{e(h),Sub\to FG}$ are the inward FG electron (hole) flux from CG and from substrate respectively.

The net flux of electrons and holes in FG results in charge loss $\Delta Q_{FG}(t)$ from the FG given by:

$$\Delta Q_{FG}(t) = A\int_0^t \left[J_{h,FG}(t) - J_{e,FG}(t) \right] dt \qquad (2)$$

Due to $\Delta Q_{FG}(t)$, potential (V) along the vertical axis through the gate stack changes with time. This is given by the Poisson equation:

$$\nabla^2 V(t) = \frac{q}{\in}\left[p(t) - n(t) + N_D - N_A \right], \qquad (3)$$

where $\in$ is the dielectric constant, p and n are the electron and hole concentration at time t and N_D and N_A are the donor and acceptor doping densities respectively.

The electron and hole fluxes at any of the FG/oxide interfaces at time t after strike is calculated by the following integral over energy:

$$J_e(t) = q\int_{E_c}^{\infty} TM_e(E_{ox}(t),E)\, n(t,E)\, \upsilon_e(t,E)\, dE \qquad (4a)$$

$$J_h(t) = q\int_{-\infty}^{E_v} TM_h(E_{ox}(t),E)\, p(t,E)\, \upsilon_h(t,E)\, dE, \qquad (4b)$$

where n, p are the concentration, and υ_e and υ_h are the velocity of the generated electrons and holes respectively along the vertical axis of cell at a given time and energy. TM_e and TM_h are the transmission probabilities of electrons and holes respectively through the oxide, respectively.

For a given oxide thickness, TM_e and TM_h are functions of E_{ox} (t) or V_{FG} (t). The Eq. (3) and (4) hence need to be solved self-consistently over time to calculate the net charge loss until the carriers relax back to thermal equilibrium. The change in V_{FG} (ΔV_{FG}) is given by:

$$\Delta V_{FG}(t) = \frac{\Delta Q_{FG}(t)}{C_T} \qquad (5)$$

where C_T is the total FG capacitance.

While Eqs. (1) – (5) completely defines the system, the key challenge is to calculate the fluxes (J) in Eq. (4). This involves exploring energy-resolved concentrations of the generated carriers during their way back to thermal equilibrium. We now explore a systematic way to do so by using numerical simulation.

IV. Model Validation By Numerical Simulations

The number of electron-hole pairs generated by a particle strike in the FG depends on the amount of energy deposited by the strike and is characterized by the particle's linear energy transfer (LET) in the material. In the case of high LET particles, e.g. heavy ions and fragments from cosmic ray neutron reactions, very dense cluster of carriers is generated due to the ionization of target atoms. The initial carrier cluster is usually modeled as a cylinder of charges with a Gaussian radial spread of ~25-50 nm in silicon [19]. Since the area of the cylinder of charges is approximately equal to the FG area in current generation Flash cells, we can approximate the whole volume of the FG with a uniform density of charges following the particle strike. The carrier dynamics and their energy distributions in the initial times after the strike before thermalization are relatively unexplored topics in literature. It is however known that the particle strike creates high energy electrons (delta rays) which can have a very broad spectrum of energy ranging from a few eV to thousands of eV. The high energy electrons lose their energy rapidly by further ionization generating more carriers in the process. Within a very short time after strike (a few fsec) almost all of the generated carriers relax to the energy range below ~10eV. After the ionization is complete, carriers lose their energy predominantly by the lattice vibrations, i.e. phonon scattering, until thermalization to the lattice temperature is complete. This second phase takes place in a time period of ~ 1 psec. Although translating the complexity of the above-mentioned phenomena in exact numerical simulation is essentially impossible because it requires complex multi-particle simulation over a large range of energy (0-1000 eV), yet much insight can be gained by judiciously chosen approximate models.

A. Initial Carrier Distribution n(E, t ⟶ 0)

We start by looking into the carrier distributions after a few fsec of strike when all the generated carriers have relaxed to <10eV energy range. For cosmic ray neutrons and other heavy ions strikes, the cluster of generated e-h pair can be described by a very dense cylinder of hot electron-hole pairs having density of the order 10^{19} cm^{-3} or higher [17]. Primary mechanisms for carrier thermalization at these high densities are collisions with other carriers, plasmons production and phonons emission. For the sake of simplicity, we can neglect the plasmons production since it is not the dominant channel of thermalization. The carrier-carrier (c-c) scattering on the other

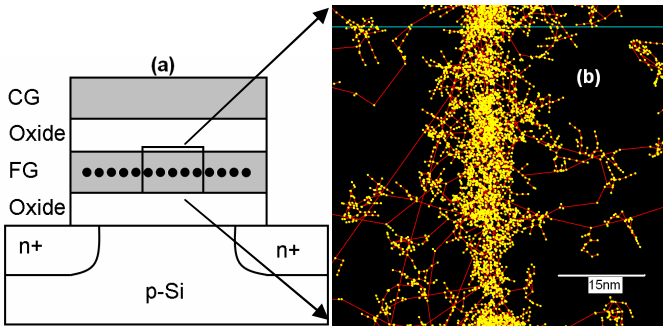

Fig. 4 (a) Cross-sectional view of a FG memory cell, (b) the primary radiation interaction of a 177 MeV Chlorine ion through the FG cell simulated in Geant4 — high energy physics based simulator for the passage of particles in matter. The region shown is the zoomed version of the region shown in (a). The electron tracks are clustered around the primary (vertical) particle track. The dots indicate a delta step to the tracks. The hierarchical structure of secondary electron generations can be observed.

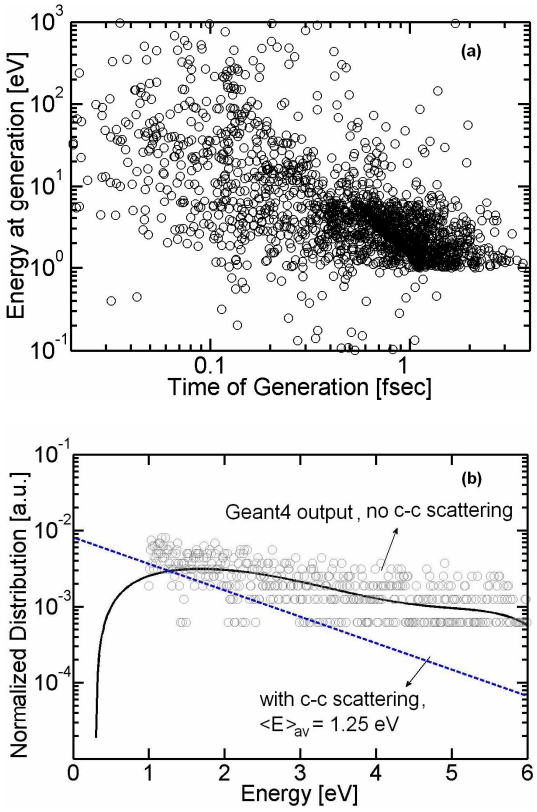

Fig. 5 (a) Initial energy of generated electrons a plotted as a function of the time of generation. The time of generation is measured as the interval between the beginning of the primary particle track and the generation of the electron (b) shows the Geant4 output distribution (solid line) compared with the Fermi-Dirac distribution which has thermalized to a very high temperature (T_e), $3/2\,k_B T_e = 1.25eV$, due to high c-c scattering. The Geant4 distribution on the other hand is relatively flat because it does not account for c-c scattering at low energies.

hand is very strong at these carrier densities having time constant of the order ~ 1 fs [20]. The c-c scattering therefore acts as a primary channel of thermalization at short time scales. The c-c scattering however does not reduce the total energy of the carriers; it only redistributes the energy among them. The carrier distribution therefore initially thermalizes to a temperature (T_e) which is much greater than the lattice temperature (T_L). The initial number of electrons, N(t = 0^+), can therefore be described by Fermi Dirac distribution with $T_e >> T_L$ (a similar equation applies for holes):

$$N(0^+) = \Omega N_c(0^+)\Im_{1/2}\left[\left(E_c - E_F(0^+)\right)/k_B T_e(0^+)\right] = \frac{LET\left[eV/\mu m\right]}{3.6eV}\times t_{FG}\left[\mu m\right] \qquad (6)$$

where $N(0^+)$ is the total number of generated carriers given by particle LET, N_c is a constant given by: $N_c(0^+) = 2\left(2\pi m^* k_B T_e(0^+)/h^2\right)^{3/2}$, $E_F(0^+)$ is the initial Fermi level, $k_B T_e(0^+)$ is the initial average electron energy, Ω and t_{FG} are total volume and thickness of FG, respectively.

In silicon, the average energy to create 1 e-h pair is about 3.6eV [17]. Assuming that all of the energy from particle strike gets transferred to the generation of electrons and holes, the initial average carrier (electron or hole) energy (<E>) should approximately be:

$$< E(0^+) >= \frac{3}{2}k_B T_e(0^+) \approx \frac{3.6-1.1}{2} = 1.25eV,$$

where 1.1eV is the silicon band-gap energy. The factor of two comes from the assumption that both electron and hole have equal average energy.

In order to validate this assumption regarding the initial carrier distribution, we simulated the primary radiation interaction by using a high-energy particle physics based toolkit – Geant4, which simulates the process of ionization and initial relaxation of generated electrons [21, 22]. We solve for the energies of primary (delta) electron tracks and those of the subsequently generated secondary electron tracks. The low energy electromagnetic package of Geant4 is used which is based on cross section data for ionization and atomic relaxation for a large energy range going down to a few eV. The data is extracted from a set of publicly distributed data libraries [23]. From Geant4 simulation we get the energy distributions of the generated electrons until the ionization phase is complete. Since the current version of Geant4 does not include all aspects of the carrier transport when the energy is very low (< 10eV), we do not use it to simulate the complete thermalization phase of carriers, but rather confine it only for a few initial fsec carrier profiling.

Fig. 4 (b) shows a two-dimensional view of hierarchy of electron trajectories from a Geant4 simulation in the FG area as shown in Fig. 4 (a). In this simulation, 177 MeV Chlorine (*Cl*) ion strikes through a FG cell normally from top of the cell. The lines that branch out of the vertical lines are tracks of primary generated electrons. The circles indicate a delta incremental step to the track. Each track has several branches which indicate the hierarchical generation of secondary electrons. Fig. 5 (a) shows the initial energy of the generated electrons *vs.* time of generation where time is measured from the start of the *Cl* ion track. The electrons have a broad spectrum of initial energy although most of them are in less than 10eV range while the time span of the ionization is ~ 3 fsec.

We get the energy distribution of the generated electrons from Geant4 when they have relaxed down to $\leq$ 6eV within a few fsec. This electron distribution is shown in Fig. 5(b). For comparison, the Fermi-Dirac distribution which we assume as our initial carrier distribution is also plotted (dotted line). Both distributions show that

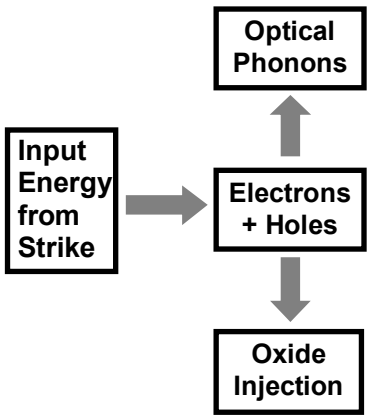

Fig. 6 The chart of energy flowing in the carriers and phonons due to a radiation dose deposited in the FG cell. The energy is first injected to electrons and holes by particle strike. A part of energy is carried away by oxide injection while the other part is lost to phonons through carrier-phonon scattering.

the carriers have a broad energy distribution with high energy tail well populated right after the ionization phase is complete. Since c-c scattering is not accounted for in Geant4, the Geant4 distribution is almost flat even at high energy.

B. Carrier Dynamics and Energy Relaxation (fsec < t < psec)

Given the initial distribution, we next consider the carrier dynamics and energy relaxation of the carrier distributions in a hydrodynamic model which is appropriate for dense electron-hole pairs in the c-c scattering dominated regime. Fig. 6 illustrates the path of energy flow in one of the FG, CG or substrate regions of the cell. The particle strike deposits energy to electrons and holes by the process of ionization. During thermalization back to the lattice temperature, the carriers can lose their energy in the following two major ways: (i) energy is lost by different scattering mechanisms predominantly by optical phonons and (ii) energy is lost because of the carriers' injection into the oxide. We calculate the former by doing Monte-Carlo simulation in the energy range 0-6eV. The latter is calculated by solving for the carrier flux over the oxide barriers by the self consistent solution of Eq. (4) and (5).

Hydrodynamic (HD) model:

We solve for the carrier relaxation from a hot thermalized distribution having $T_e >> T_L$ back to thermal equilibrium i.e. $T_e = T_L$ in the FG region using hydrodynamic model (CG and substrate regions are similarly modeled). We assume that generated carriers have a uniform density in the FG. The following rate equations for the total number of electrons (N) and their total energy (E) in the FG can be written (similar equations can be written for holes):

$$dN/dt = -AJ_{e,FG}(t)/q \qquad (7)$$

$$dE/dt = -A\left[J_{E,in}(t) - J_{E,out}(t)\right]/q - E_{ph}(t) \qquad (8)$$

where $J_{e,FG}$ is the net FG electron flux defined in Eq. (4) while $J_{E,in}(t)$ and $J_{E,out}(t)$ are the energy flux due to the flow of electrons in and out of the FG respectively. $E_{ph}(t)$ is the energy lost to scattering mechanisms predominantly with optical phonons and A is the FG area.

In typical HD models, an energy independent carrier relaxation time due to phonon scattering is used. This is however considered as one of the main limitations of HD models. We use Monte Carlo simulations to calculate E_{ph} in order to properly account for the carrier relaxation due to phonons and other scattering mechanisms in the lower energy range (0 – 6 eV). The shape of the carrier distributions is still assumed to be Fermi-Dirac because of high c-c scattering.

Energy Loss to Phonons—Monte Carlo Method:

We use a full-band ensemble Monte Carlo simulator in the lower energy range (0—6eV), which is described in [24]. The Monte Carlo simulation included phonon scattering, ionized impurity scattering and impact ionization. We use an approach called Transition matrix approach (TMA) to solve the time dependant but space independent Boltzmann equation for distribution function (f):

$$\partial f/\partial t = S_{op} f = \sum_{p'} f(p')S(p',p)\left[(1-f(p))\right] - f(p)S(p,p')\left[(1-f(p'))\right]$$

where S is the scattering operator, p and p' are the current and the outgoing momentum states respectively [25]. The TMA is a table based Monte Carlo approach which is used to reduce a large computational time and the statistical noise of a direct Monte Carlo simulation. In TMA the scattering probabilities are pre-computed and tabulated. The transition matrix (T) is a square matrix in which each element (T_{ij}) represents the probability of carrier transition from an input energy (E_j) to output energy (E_i) in a short time step (Δt).

We pre-computed the elements T_{ij} by running the direct Monte Carlo simulation in which 50000 electrons were launched at random locations on the isoenergy surfaces for a given energy (E_j) and the subsequent relaxation is observed for Δt=10fs. $T_{ij} = N_j / N_i$, where N_j and N_i are the number of carriers in the output and input energy bins respectively. Once the transition matrix is constructed the carrier relaxation due to phonon scattering can simply be calculated by the matrix multiplication: $f_{ph}(t) = T_{ij} \times f_{c-c}(t)$, where $f_{c-c}(t)$ is the Fermi-Dirac distribution due to c-c scattering and $f_{ph}(t)$ is the relaxed carrier distribution due to phonon and other above mentioned scattering mechanisms. The total energy loss during this relaxation (ΔE_{ph}) is calculated as:

$$\Delta E_{ph}(t) = N_c(t)\int_E E\left[f_{c-c}(t) - f_{ph}(t)\right]dE$$

$\Delta E_{ph}(t)$ from the above equation is then fed back to Eq. 8.

Fig. 7 shows the electron distribution functions in FG as a function of time. The solid lines represent the relaxation of electron distributions at given times due to the combined effect of phonon scattering and electron flux over the oxide barriers. These distributions however rapidly get thermalized to T_e (t) since c-c scattering rate is strong. The thermalized distributions are shown in dotted line in Fig. 7. It should be noted that high energy tail remains populated for ~100 fsec.

The phonon scattering and the carrier flux over the oxides reduce the average carrier energy $k_B T_e$. At any time t, $k_B T_e$ can be calculated as [20]:

$$< E > (t) = \frac{3}{2} k_B T_e(t) \frac{\Im_{3/2}(\eta)}{\Im_{1/2}(\eta)} = \frac{E(t)}{N(t)} \qquad (9)$$

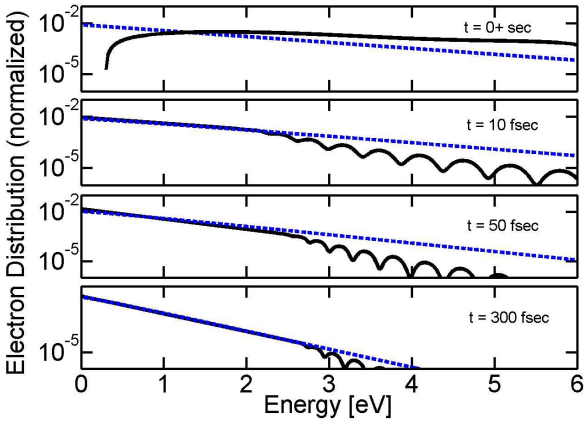

Fig. 7 Electron energy distributions as a function of time. The solid lines are the distributions obtained from contributions of (i) carrier relaxation in Monte Carlo simulation and (ii) the oxide injection. The dotted curves are the assumed Fermi-Dirac distributions which are the result of high carrier-carrier scattering.

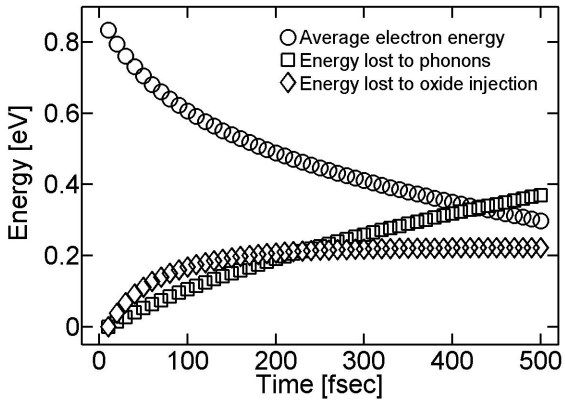

Fig. 8. The average electron energy as a function of time after the particle strike. The energy drops due to phonon scattering and the oxide injection.

where $\Im_{3/2}(\eta)$ and $\Im_{1/2}(\eta)$ are the Fermi-Dirac integrals of order 3/2 an 1/2 respectively. $\eta = (E_F - E_c)/k_B T_e$. Fig. 8 shows the average electron energy (~ $k_B T_e$) in the FG as a function of time. The energy lost to phonons and oxide fluxes are also plotted. The average energy decreases while carriers lose their energy to phonons and oxide fluxes. It should be noted that average electron energy is still much greater than the average carrier energy at equilibrium with lattice ($k_B T_L$ =26meV), for more than 500 fsec.

V. Results

Having developed a detailed model for carrier fluxes J(t), we can now use it to calculate the amount of charge loss in FG cells due to particle strikes. We use a FG cell having dimensions of W × L × t_{FG} = 100nm × 100nm × 50nm for charge loss calculations. Fig. 9 shows the incoming and outgoing carriers at the FG/tunnel oxide interface as a function of time after the strike. Because of the electric field, number of outgoing FG electrons is much higher than the incoming FG electrons during the initial times. The opposite is true for the holes. The number of holes at any time is however much smaller than that of electrons because holes have a higher energy

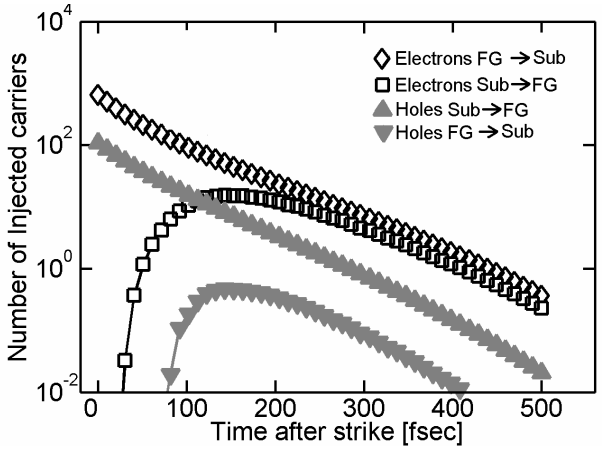

Fig. 9 The number of electrons and holes injected into and out of the FG as a function of time after the particle strike.

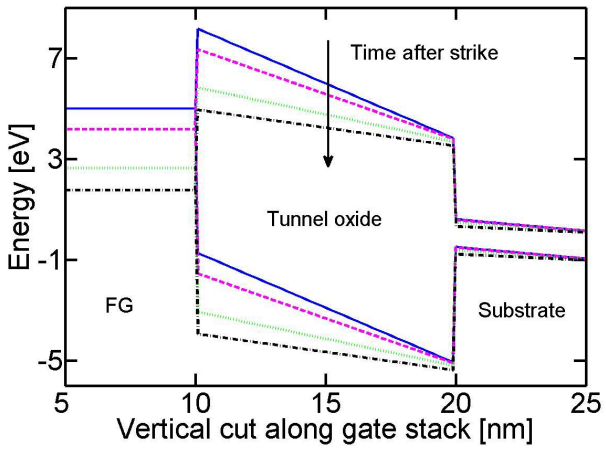

Fig. 10 The energy band profile along the vertical cut in the gate stack direction as a function of time. The FG potential and E_{ox} decrease with time due to loss of stored electrons in FG.

barrier. The net flow of electrons out of the FG reduces V_{FG} and the oxide field as a function of time. This is illustrated in Fig. 10. The Fig. shows the energy band profiles at the FG/tunnel oxide interface along the vertical axis of the cell for various times. Due to the decrease of E_{ox}, the inward and outward FG electrons become almost equal at later times as shown in Fig. 9.

Fig. 11 shows the total number of electron loss from the FG as a function of prestrike oxide electric field in the programmed state. The simulation results for different particle LETs are plotted (open symbols). The curves match reasonably well with the data from Ref. [15] (closed symbols). Since we did not know the FG area of the Flash cells of [15], we calibrated our simulation results by a constant factor (~ 0.7) for all LETs in order to compare with the experimental data.

In Fig. 12, we plot the total number of electron loss from the FG as function of particle LET. The two curves correspond to two different prestrike oxide electric fields in the programmed state. The experimental data from Ref. [15] is also plotted (closed symbols) which matches well with simulation results (open symbols). It is interesting to note that for alpha particles (LET~1.5MeV-cm^2/mg) and typical cosmic ray neutrons recoils (LET ~ 5-15 MeV-cm^2/mg)

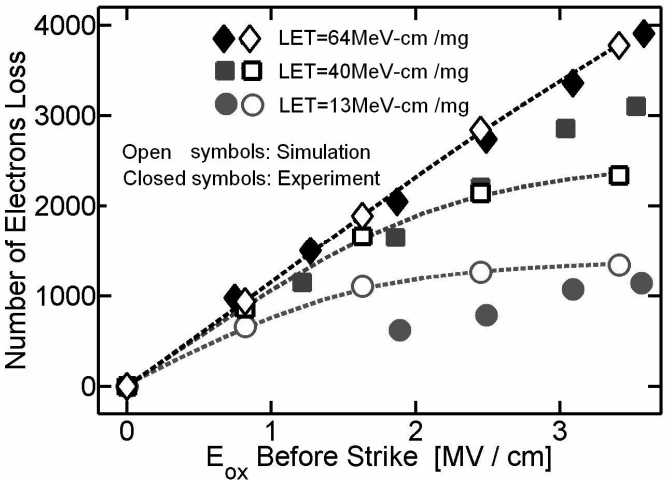

Fig. 11 Number of electrons loss as a function of E_{ox} for particle strikes having different LETs. The number of electron loss goes up with increasing E_{ox} because the *net* electron flux out of FG increases with higher E_{ox}.

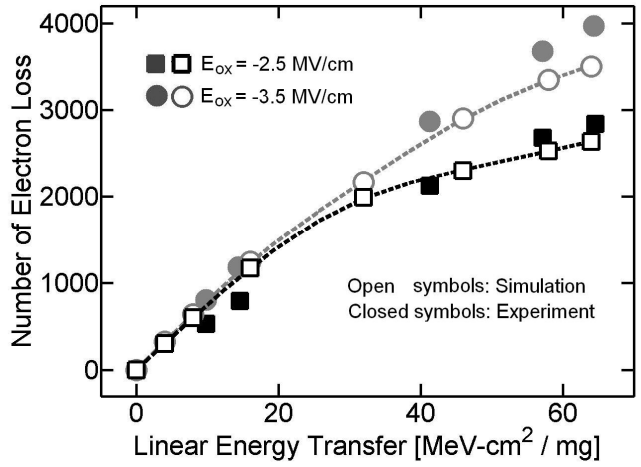

Fig. 12 Number of electron loss as a function of particle LETs at two different oxide electric fields. The number of electron loss goes up with increasing LET because more carriers are produced as LET is increased which increases the *net* electron flux out of FG.

the charge loss is on the order of 100-500 electrons, respectively. For typical current generation FG memory cells which store ~1000 or fewer electrons, this is a considerable charge loss which may directly cause a SEU or (at the very least) significantly reduce the noise margin (programming window) between the memory states.

We plot the stored charge in the programmed state and the charge loss tolerance for various technology generations of NAND Flash memory cells in Fig. 13 [3]. For single level Flash cells (SLC), charge loss tolerance can be up to 20%, while for multi level cells (MLC), it can be assumed to be 5% of the total stored charge. The figure also shows the predicted charge loss for cosmic ray neutrons and alpha particles at E_{ox}=3MV/cm from our simulation (solid symbols). For SLC, the predicted number of FG electron loss by cosmic ray neutron and alpha particle strikes are indeed above the charge loss tolerance limit of NAND Flash technologies below 70nm and 50nm nodes respectively. For MLC, the loss tolerance for 90nm node is already below the predicted charge loss from cosmic ray neutron strikes while sub 80nm nodes are below the charge loss value due to alpha particles.

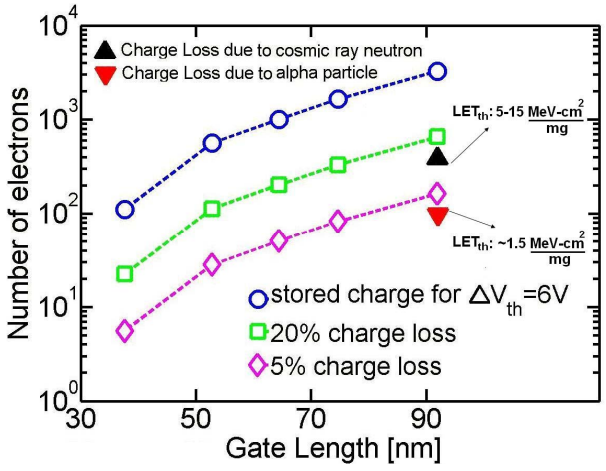

Fig. 13 Number of electron stored in NAND Flash cell (circles) and charge loss tolerance as a function of FG technology design rule. The charge loss tolerance of SLC is assumed to be 20 % (squares), while that of MLC is taken as 5% (diamonds). The predicted charge loss due to cosmic ray neutrons and alpha particle strikes (solid symbols) at E_{ox}=3MeV/cm is shown for comparison. The stored charge and the loss tolerance rapidly reduce with cell scaling which greatly increases the SEU sensitivity of the cells.

TABLE I
SUMMARY OF SEU TESTS IN HIGH DENSITY NAND FLASH MEMORIES FROM DIFFERENT EXPERIMENTS

Flash Memory Arrays [Size/Technology]	Threshold LET [MeV-cm²/mg]	Saturation Cross-section [cm²/bit]
4 Gb/90nm [7]	3.4	6×10^{-11}
2 Gb/90nm [27]	12	5×10^{-13}
1 Gb/90nm [28]	No data	6×10^{-11}
1Gb/No data [29]	5	1×10^{-10}
4Gb/63nm [26]	3.5	5×10^{-11}

VI. DISCUSSION

Our analysis in the previous section highlights a number of very interesting trends in the SEU sensitivity of future FG memories, though the exact quantitative values might vary depending upon the cell parameters like area, coupling ratios, *etc*. It is evident that the cell scaling is expected to greatly affect the radiation hardness of future FG memories. Although there is not much data available to validate our predictions for highly scaled FG cells, we provide a summary of some of the recent experiments done on commercial high density NAND Flash memories in Table I. The threshold LET (LET_{th}) to upset a FG cell made in 90nm technology node is between 3 – 12 MeV-cm²/mg as shown in the Table I. This is indeed in agreement with our simulation results in Fig. 13 where the SLC charge loss tolerance is just above the charge loss calculated for cosmic ray neutron strikes (LET ~ 5 – 15 MeV-cm²/mg). The reported saturation cross-sections of 90/65 NAND Flash memories are of the order of 10^{-13} – 10^{-10} cm²/bit making them suitable for use in many of the radiation harsh environments e.g. in space

applications, provided proper error detection and correction (EDAC) schemes are used. The LET_{th} in future FG memories is however expected to reduce significantly as we illustrate in Fig. 13 and their suitability for radiation harsh environments will have to be carefully revaluated.

VII. Conclusions

We proposed TCF model for charge loss due to SEU in FG memory cells. A dense cluster of hot electron-hole pairs is generated after a particle strike with carriers having broad energy distributions which relax back to thermal equilibrium in a time ~ 1 psec. The tail of the high energy distribution results in a transient carrier flux into and out of the FG over the tunnel and inter-poly oxides. In the programmed cell state, oxide electric field favors the flow of electrons out of the FG. This makes the electron flux out of the FG greater than that coming into the FG, causing a net loss in the stored FG electrons. We use numerical simulations to validate the TCF model. A high-energy particle physics based toolkit – Geant4 is used to validate the generation and initial energy distributions in the high energy range (~10eV— ~ keVs). For carrier relaxation in low energy (< 10eV) range, we used hydrodynamic model which is coupled with Monte Carlo simulations in order to correctly account for energy relaxation due to phonon scattering and impact ionization. The transient hot carrier flux into and out of the FG over the oxides barriers are calculated by solving for the transmission probability through the oxides self consistently with the Poisson equation, until the carriers relax back to thermal equilibrium. Finally, we estimated the amount of charge loss in Flash memory cells due to alpha particles and cosmic ray neutron strikes. We predicted that Flash memory cells, which were previously considered to be relatively immune to SEU, can become highly sensitive to SEU in future due to rapidly decreasing charge loss tolerance (~ 10-100 electrons).

Acknowledgements

The authors would like to thank P. D. Yoder for his help in Monte Carlo simulations.

References

[1] P. Cappelletti, C. Golla, P. Olivo, and E. Zanoni, *Flash Memories*: Kluwer Academic Publishers, 1999.

[2] P. Pavan, R. Bez, P. Olivo, and E. Zanoni, "Flash memory cells-an overview," *Proceedings of the IEEE*, vol. 85, pp. 1248-71, 1997.

[3] S. YunSeung, "Non-volatile memory technologies for beyond 2010," Kyoto, Japan, 2005.

[4] G. Molas, D. Deleruyelle, B. De Salvo, G. Ghibaudo, M. Gely, S. Jacob, D. Lafond, and S. Deleonibus, "Impact of few electron phenomena on floating-gate memory reliability," *Electron Devices Meeting, 2004. IEDM Technical Digest. IEEE International*, pp. 877-880, 2004.

[5] G. Cellere, P. Pellati, A. Chimenton, J. Wyss, A. Modelli, L. Larcher, and A. Paccagnella, "Radiation effects on floating-gate memory cells," *Nuclear Science, IEEE Transactions on*, vol. 48, pp. 2222-2228, 2001.

[6] G. Cellere, A. Paccagnella, A. Visconti, M. Bonanomi, S. Beltrami, J. R. Schwank, M. R. Shaneyfelt, and P. Paillet, "Total Ionizing Dose Effects in NOR and NAND Flash Memories," *Nuclear Science, IEEE Transactions on*, vol. 54, pp. 1066-1070, 2007.

[7] F. Irom and D. N. Nguyen, "Single Event Effect Characterization of High Density Commercial NAND and NOR Nonvolatile Flash Memories," *Nuclear Science, IEEE Transactions on*, vol. 54, pp. 2547-2553, 2007.

[8] F. Irom, T. F. Miyahira, D. N. Nguyen, I. Jun, and E. Normand, "Results of Recent 14 MeV Neutron Single Event Effects Measurements Conducted by the Jet Propulsion Laboratory," *Radiation Effects Data Workshop, 2007 IEEE*, 2007.

[9] G. Cellere, L. Larcher, A. Paccagnella, A. Visconti, and M. Bonanomi, "Radiation induced leakage current in floating gate memory cells," *Nuclear Science, IEEE Transactions on*, vol. 52, pp. 2144-2152, 2005.

[10] G. Cellere, A. Paccagnella, A. Visconti, and M. Bonanomi, "Secondary Effects of Single Ions on Floating Gate Memory Cells," *Nuclear Science, IEEE Transactions on*, vol. 53, pp. 3291-3297, 2006.

[11] G. Cellere, A. Paccagnella, A. Visconti, M. Bonanomi, and A. Candelori, "Transient conductive path induced by a Single ion in 10 nm SiO_2 Layers," *Nuclear Science, IEEE Transactions on*, vol. 51, pp. 3304-3311, 2004.

[12] G. Cellere, L. Larcher, A. Paccagnella, A. Visconti, and M. Bonanomi, "Radiation induced leakage current in floating gate memory cells," *IEEE Transactions on Nuclear Science*, vol. 52, pp. 2144-52, 2005.

[13] G. Cellere, A. Paccagnella, L. Larcher, A. Chimenton, J. Wyss, A. Candelori, and A. Modelli, "Anomalous charge loss from floating-gate memory cells due to heavy ions irradiation," Phoenix, AZ, USA, 2002.

[14] G. Cellere, A. Paccagnella, A. Visconti, and M. Bonanomi, "Soft errors induced by single heavy ions in floating gate memory arrays," Monterey, CA, USA, 2005.

[15] G. Cellere, A. Paccagnella, A. Visconti, and M. Bonanomi, "Subpicosecond conduction through thin SiO layers triggered by heavy ions," *Journal of Applied Physics*, vol. 99, pp. 074101, 2006.

[16] G. Cellere, A. Paccagnella, A. Visconti, M. Bonanomi, and A. Candelori, "Transient conductive path induced by a Single ion in 10 nm SiO_2 Layers," *IEEE Transactions on Nuclear Science*, vol. 51, pp. 3304-11, 2004.

[17] T. M. Ma and P. V. Dressendorfer, "Ionization Radiation E! ects in MOS Device and Circuit," Wiley, New York, 1989.

[18] E. S. Snyder, P. J. McWhorter, T. A. Dellin, and J. D. Sweetman, "Radiation response of floating gate EEPROM memory cells," Marco Island, FL, USA, 1989.

[19] P. Oldiges, R. Dennard, D. Heidel, B. Klaasen, F. Assaderaghi, and M. Ieong, "Theoretical determination of the temporal and spatial structure of α-particle induced electron-hole pair generation in silicon," Reno, NV, USA, 2000.

[20] E. J. Yoffa, "Dynamics of dense laser-induced plasmas," *Physical Review B (Condensed Matter)*, vol. 21, pp. 2415-25, 1980.

[21] M. Asai, "Geant4-a simulation toolkit," *Transactions of the American Nuclear Society*, vol. 95, pp. 757, 2006.

[22] J. Apostolakis and D. H. Wright, "An overview of the Geant4 toolkit," Batavia, IL, USA, 2007.

[23] S. Chauvie, S. Guatelli, V. Ivanchenko, F. Longo, A. Mantero, B. Mascialino, P. Nieminen, L. Pandola, S. Parlati, L. Peralta, M. G. Pia, M. Piergentili, P. Rodrigues, S. Saliceti, and A. Tnndade, "Geant4 low energy electromagnetic physics," Rome, Italy, 2004.

[24] P. D. Yoder, M. I. Vexler, A. F. Shulekin, N. Asli, S. V. Gastev, I. V. Grekhov, P. Seegebrecht, S. E. Tyaginov, and H. Zimmermann, "Luminescence spectra of an Al/SiO_2/p-Si tunnel metal-oxide-semiconductor structure," *Journal of Applied Physics*, vol. 98, pp. 83511-1, 2005.

[25] M. A. Alam and M. S. Lundstrom, "Transition matrix approach for Monte Carlo simulation of coupled electron/phonon/photon dynamics," *Applied Physics Letters*, vol. 67, pp. 512-14, 1995.

[26] T. R. Oldham, T. R. Oldham, M. Friendlich, J. W. Howard, M. D. A. B. M. D. Berg, H. S. A. K. H. S. Kim, T. L. A. I. T. L. Irwin, and K. A. A. L. K. A. LaBel, "TID and SEE Response of an Advanced Samsung 4Gb NAND Flash Memory TID and SEE Response of an Advanced Samsung 4Gb NAND Flash Memory," presented at Radiation Effects Data Workshop, 2007 IEEE, 2007.

[27] T. R. Oldham, T. R. Oldham, R. L. Ladbury, M. Friendlich, H. S. A. K. H. S. Kim, M. D. A. B. M. D. Berg, T. L. A. I. T. L. Irwin, C. A. S. C. Seidleck, and K. A. A. L. K. A. LaBel, "SEE and TID Characterization of an Advanced Commercial 2Gbit NAND Flash Nonvolatile Memory SEE and TID Characterization of an Advanced Commercial 2Gbit NAND Flash Nonvolatile Memory," *Nuclear Science, IEEE Transactions on*, vol. 53, pp. 3217-3222, 2006.

[28] M. Bagatin, G. Cellere, S. Gerardin, A. Paccagnella, A. Visconti, S. Beltrami, and M. Maccarrone, "Single Event Effects in 1Gbit 90nm NAND Flash Memories under Operating Conditions Single Event Effects in 1Gbit 90nm NAND Flash Memories under Operating Conditions," presented at On-Line Testing Symposium, 2007. IOLTS 07. 13th IEEE International, 2007.

[29] T. E. Langley, T. E. Langley, and P. Murray, "SEE and TID test results of 1 Gb flash memories SEE and TID test results of 1 Gb flash memories," presented at Radiation Effects Data Workshop, 2004 IEEE, 2004.